Lasers in Manufacturing Conference 2015

Theoretical Analysis of Laser Cutting of Metals at 1 and 10 µm wavelength

Michael H. Brügmann, Thomas Feurer

Institute of Applied Physics, University of Bern
Sidlerstrasse 5, CH-3012 Bern, Switzerland

Abstract

We present a theoretical analysis of laser cutting of metals based on a model originally proposed by Niziev and an extension which includes heat conduction. Specifically, we investigate the dependence of relevant parameters, such as maximum cutting speed, shape of the cutting front et cetera, on wavelength, polarization, and laser beam properties. A special emphasis is on the comparison between results obtained for lasers around 1 µm and CO_2 lasers at 10 µm wavelength, respectively. To test the model we compare the numerical solutions for a cold-work steel work-piece to experimental results presented elsewhere. We find good agreement between theoretical and experimental observations. The main differences between laser cutting with 1 and 10 µm lasers arise from the different absorptivity profiles and absorbed intensities. In most of the analysed cases the computed mean absorbed intensities as well as the absorbed intensity profiles show that the energy transfer is more efficient for laser cutting with 1 µm lasers.

Keywords: Macro-Processing; Cutting; Solid-State Laser; CO_2-Laser

1. Introduction

In the last years several theoretical and experimental studies investigating solid-state laser (i.e., disk or fiber lasers operating around 1 µm wavelength) inert gas fusion cutting have been carried out. Experiments

revealed distinct differences with respect to the standard CO_2 laser beam fusion cutting process. Specifically, the maximum speed for disk and fiber laser cutting of metal sheets is usually higher than for CO_2 laser cutting given the same laser power output level [1]. Moreover, the high cut edge quality in CO_2 laser cutting, with almost regular striation patterns, has not yet been achieved in fiber and disk laser cutting of work pieces with thicknesses greater than 5 mm [2]. Until now there is not a clear explanation for these particular differences between CO_2 and solid-state laser cutting. In the past, theoretical analysis has focused on the wavelength dependent absorptivity at the cutting front [3], the absorbed intensity [4], and the role of multiple reflections and its effects on the cutting front as well as on the cutting edges [5]. Also, hydrodynamic, mechanical, and thermal phenomena, such as the hydrodynamics of the melt layer [2], [6], [7], [8], the melt removal from the cut kerf [9], [10], the effect of a high recoil pressure [11], and the temperature at the cutting front [12], were investigated in view of their influence on the cut quality. Here, we analyze the differences observed in laser inert gas fusion cutting with the help of model originally proposed by Niziev [13] and extended to include heat conduction [14].

2. Mathematical modeling and physical parameters

In references [13], [15] V.G. Niziev and A. Nesterov presented a theory of continuous wave laser cutting. Recently, we have shown that this formalism can be derived from a local energy balance [14] and have extended it in order to incorporate heat conduction from the kerf to the bulk material. Solutions can be found by splitting the resulting equation in a stationary and a time-dependent part [13], [15], [14]. The solution to the stationary part is computed in the laser's moving coordinate system and yields the shape of the cutting profile. Generally, there are no exact solutions to the nonlinear differential equation and we have to resort to numerical methods. In order to compare the numerical solutions to a recently published comparative experimental study, we performed the computations for the laser cutting parameters and material parameters as given in reference [1]. In this reference a CO_2 laser and a disk laser were used to cut cold-work tool steel 90MnCrV8 (AISI O2) plates with thicknesses of 5 mm and 8 mm. All experiments were carried out with an average laser power of 3 kW. We approximate both laser beams by Super-Gauss beams [14] with M^2 calculated from [16]. Both lasers emitted unpolarized beams.

3. Results and Analysis

A large number of publications [17], [18], [19] experimentally investigate CO_2 laser cutting and more recent publications [1], [10], [11] [20] started to present results at 1.03 µm. Here, we compare our theoretical model to experiments published on a comparative study of inert gas fusion cutting of 5 mm and 8 mm thick 90MnCrV8 work pieces at 1.03 µm and 10.6 µm, respectively [1]. Specifically, we investigate the maximum cutting speed as a function of focus position and material thickness and analyze the shape of the cutting profile.

3.1 Maximum cutting speed

The maximum cutting speed is defined as the speed for which the calculated cutting profile is just deep enough to cut through a work piece of a given thickness. One of the main observations in reference [1] is that the maximum cutting speed is generally higher for the disk laser, decreases with material thickness, and depends on the position of the beam focus. Figures 1 and 2 show the simulated cutting speed as a function of the relative focal position f/d for a 5 mm and 8 mm thick work piece. The upper surface corresponds to f/d=0 and the lower surface to f/d=-1, respectively.

We start with the original Niziev model. An important result is that the highest cutting speeds for the disk as well as for the CO_2 laser are achieved when the focal position is at the middle of the work piece, i.e. for f/d ≈ -0.5 (see Figs. 10 and 2(a)). Further, the maximum cutting speed for the disk laser is almost always larger than for the CO_2 laser (see Figs. 1(a) and 2(a)). If the focal position is at the middle of the work piece our computations indicate a higher maximum cutting speed for the CO_2-laser. All of these results are in qualitative agreement with the experiments, however, the quantitative agreement is rather poor. For example our theoretical results for f/d=-0.33 and f/d=-0.66 are by a factor of two to five higher than the experimental values. Despite the differences in absolute values it is worthwhile noting that the ratio of the maximum cutting speeds of the two laser sources is between one and two, which is in good agreement with the experimental observations. We attribute the quantitative differences to mainly two effects. First, the refractive index and the extinction coefficient were estimated by means of Drude's theory. Since the 90MnCrV8 work piece is an alloy, the values for n and κ are only approximately correct. Second, the ejected molten layer from the cutting front and the heat conductivity in the bulk material are neglected. They affect the energy balance since they both transport energy away from the kerf. Both reduce the amount of energy disposable for the melting process and, as a consequence, the cutting speed is reduced.

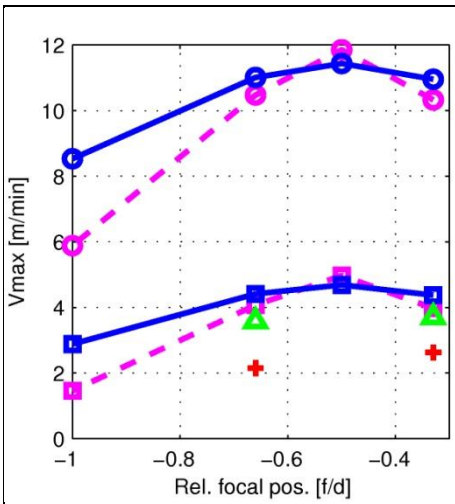

(a): Maximum cutting speed as function of the focal position for a 5 mm thick work piece: magenta dashed curves: CO_2-laser, blue solid curve: disk laser, circles: basic model, squares: extended model. The experimental values from [1] for the CO_2-laser (red cross) and the disk laser (green triangles).

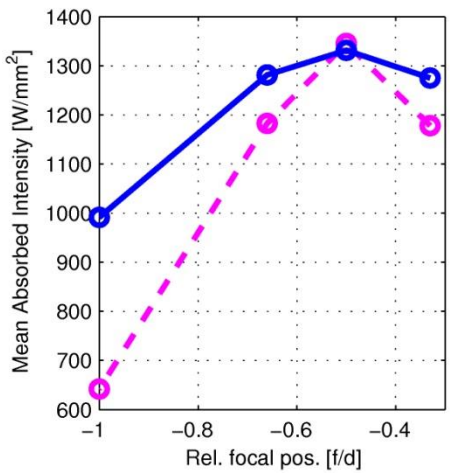

(b): Mean absorbed intensity as function of the focal position for a 5 mm thick work piece calculated from the extended model. Legend: magenta dashed curve: CO_2-laser, blue solid curve: disk laser.

Figure 1: Maximum cutting speeds and mean absorbed intensities for the 5 mm thick work piece.

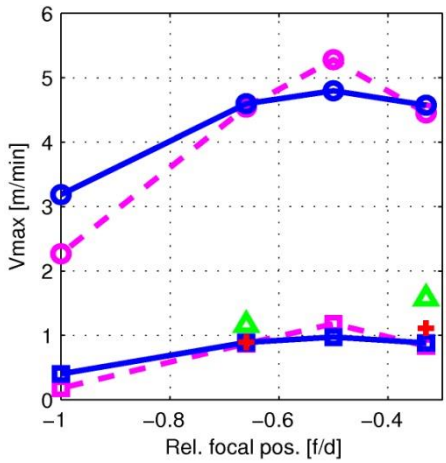

(a): Maximum cutting speed as function of the focal position for an 8 mm thick work piece: magenta dashed curve: CO_2-laser, blue solid curve: disk laser, circles: basic model, squares: extended model. The experimental values from [1] for the CO_2-laser (red cross) and the disk laser (green triangles).

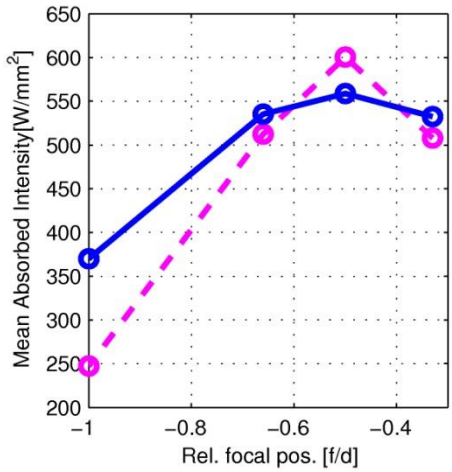

(b): Mean absorbed intensity as function of the focal position for an 8 mm thick work piece calculated from the extended model. Legend: magenta dashed curve: CO_2-laser, blue solid curve: disk laser.

Figure 2: Maximum cutting speeds and mean absorbed intensities for the 8 mm thick work piece.

Next, we use the extended model, that is, we include heat conduction to the bulk material. For comparison, these simulations are also shown in Figs 1(a) and 2(a). Obviously the net effect of the heat conductivity to the bulk is a lowering of the cutting speed for both lasers by a factor between 3 and 5. That is, by including heat conduction the quantitative agreement between the model and the experimental observations improves and is excellent especially for the 8 mm thick work piece. For the 5 mm thick work piece we find that some of the computed cutting speeds are somewhat higher than the measured ones, nevertheless, the agreement is substantially better than for the basic model.

In order to analyze the effectiveness of the energy transfer from the laser beam to the work piece, we computed the mean absorbed intensity <I>. It is obtained by dividing the line integral of the absorbed intensity along the cutting profile by the length of the cutting profile. The mean absorbed intensities as function of the focal position are depicted in Figs. 1(b) and 2(b) and the general dependence is similar for both lasers. For focal positions closer to the top or the bottom surface the mean absorbed intensity for the disk laser is always higher. This is the main reason why the cutting speeds for the disk laser are larger than for the CO_2 laser. Only for focal positions located around the middle of the work piece the absorbed intensity can be higher for the CO_2 laser. Comparing the curves of the mean absorbed intensities to the corresponding curves of the maximum cutting speeds suggests, not surprisingly, that the cutting speeds are directly proportional to the mean absorbed intensities. It is worthwhile mentioning that the mean absorbed intensities are virtually identical in both models. Figure 3(a) shows the computed maximum cutting speed as a function of thickness when the focal position is at the middle of the work piece. The model predicts a higher performance of the disk laser up to 5 mm, as can be seen by inspecting the difference in cutting speeds shown in Fig. 3(b). This advantage disappears for thicker work pieces. Both findings are in good

agreement with the experiments (see Ref. [20]and references therein). Comparing the results of the basic and the extended model shows the same overall trend (see Fig. 3(b)), however, the absolute cutting speeds resulting from the extended model are smaller (see Fig. 3(a)).

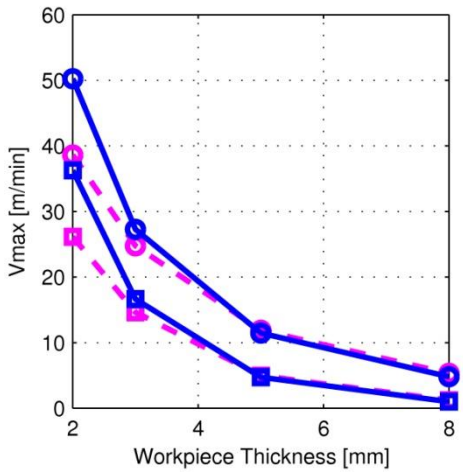

(a): Maximum cutting speed as function of the work piece thickness. Focal position f/d=-0.50. Legend: magenta pecked curve: CO_2-laser, blue solid curve: disk laser, circles: basic model, squares: extended model.

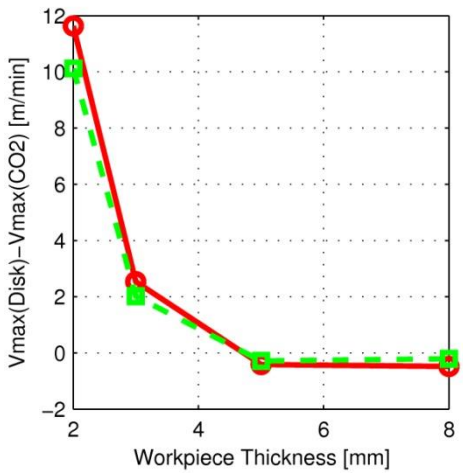

(b): Difference of the maximum cutting speed as function of the work piece thickness. Focal position f/d=-0.50. Legend: red solid line, circles: basic model, green pecked line, squares: extended model.

Figure 3: Maximum cutting speed as function of the work piece thickness.

The different results from the two models, specifically with respect to the maximum cutting speed, suggest that heat conduction losses are substantial and must not be neglected. Figures 4(a) and (c) show the heat conduction flux and Figs. 4(b) and 4(d) the heat conduction flux relative to the absorbed intensity for the 5 mm and 8 mm thick work pieces. The conductive losses with respect to the absorbed intensities are substantial for both lasers irrespective of work piece thickness. For example, for an 8 mm thick work piece over 80% of the absorbed intensity is removed through heat conduction and does not contribute to the removal of material. The conductive losses are almost always larger for the CO_2 laser than they are for the disk laser. Only when the focal position is around the middle of the work piece, i.e. f/d ≈-0.5, the situation is reversed. Also, the conductive losses increase with decreasing cutting speed which is a consequence of the dependence of the generalized ablation energy density on the Peclet number. Since the absorbed laser intensity is only a fraction of the incoming laser intensity the conductive losses for the 5 mm thick work piece, when compared to the incoming intensity, are between 21 % and 33 % for the CO_2 laser and between 28% and 36% for the disk laser. In the case of the 8 mm thick work piece the corresponding losses lie between 10% and 20% for the CO_2 laser and between 15% and 20% for the disk laser. These values are in good agreement with the conductive losses reported in references [12] and [21].

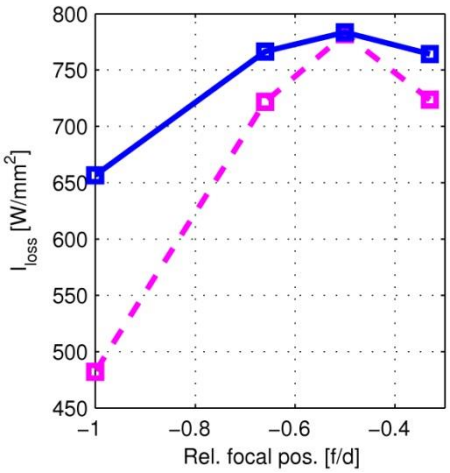

(a): Heat conduction losses as function of the focal position for a 5 mm thick work piece. Legend: magenta dashed curves: CO_2-laser, blue solid curve: disk laser.

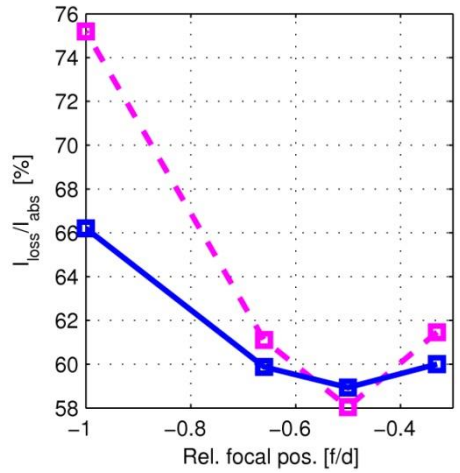

(b): The conductive losses relative to the absorbed intensities as function of the focal position for a 5 mm thick work piece. Legend: magenta dashed curve: CO_2-laser, blue solid curve: disk laser.

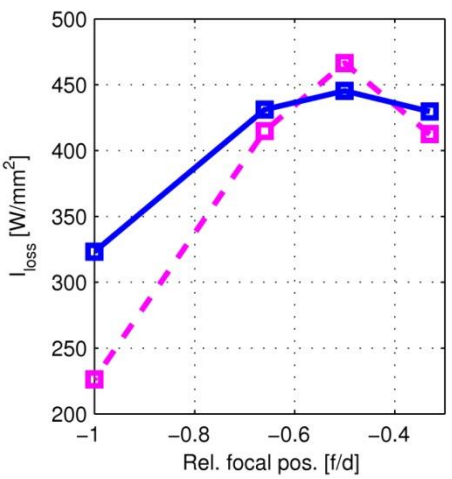

(c): Heat conduction losses as function of the focal position for an 8 mm thick work piece. Legend: magenta dashed curves: CO_2-laser, blue solid curve: disk laser.

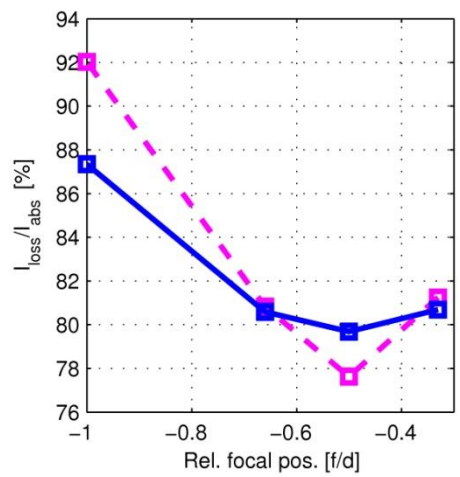

(d): The conductive losses relative to the absorbed intensities as function of the focal position for an 8 mm thick work piece. Legend: magenta dashed curve: CO_2-laser, blue solid curve: disk laser.

Figure 4: Heat conduction losses for the 5 mm and 8 mm thick work pieces.

3.2 Cutting profiles

In this subsection we compare the computed cutting and absorptivity profiles for a 5 mm thick 90MnCrV8-workpiece to the experimental results in reference [1]. Figures 5(a) and 5(b) show the calculated cutting profiles for the focal positions f/d=-0.33 and f/d=-0.66, respectively.

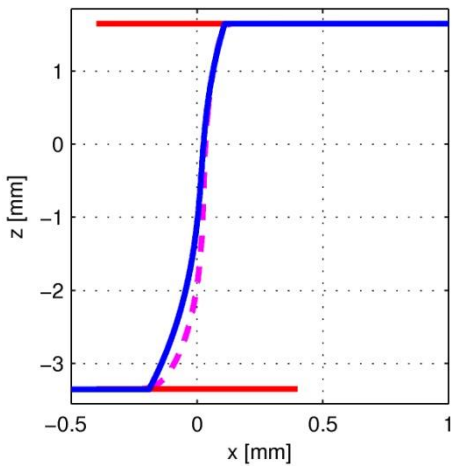

(a): Cutting profiles. Focal position f/d=-0.33. Legend: magenta pecked curve: CO_2-laser, blue solid curve: disk laser. The red lines mark the top and bottom edges of the work piece.

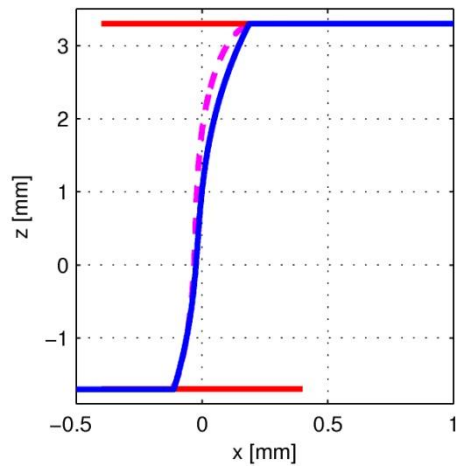

(b): Cutting profiles. Focal position f/d=-0.66. Legend: magenta pecked curve CO_2-laser, blue solid curve: disk laser. The red lines mark the top and bottom edges of the work piece.

Figure 5: Cutting profiles for a 5 mm thick 90MnCrV8 work piece.

By visual inspection of the shape of the computed and the measured cutting profiles as presented in reference [1] we find a very good qualitative agreement. Figures 5(a) and 5(b) also suggest that for a focal position of f/d=-0.33 the cutting profiles for disk and CO_2-laser differ more on the lower part of the work piece while for the f/d=-0.66 the differences are more pronounced at the upper part of the work piece. In order to compare the calculated cutting profiles to the measured ones in a more quantitative way we determine the projected longitudinal extension of the cutting profile ΔL. It is defined as (see also reference [1]) the distance between the start point on the top surface and the end point on the bottom surface of the cutting profile. The experimental and the computed values for ΔL are summarized in Table 1.

Table 1: Projected longitudinal extension of the cutting profile for a focal position f/d=-0.33.

Laser	ΔL [mm] (theory)	ΔL [mm] (experiment)
CO_2	~0.421	~0.750
Disk	~0.301	~0.500
ratio	~1.40	~1.50

While the computed values ΔL, on an absolute scale, are too low by about a factor of two, the computed ratio $\Delta L_{CO2} / \Delta L_{disk}$ is in excellent agreement with the experimental result. There are several reasons which might be responsible for the discrepancies observed when comparing absolute numbers. First, there are experimental uncertainties, e.g. the cutting profile after switching off the laser and the gas flow might not be identical to the one during the cutting process. Second, the model is based on several approximations which affect the cutting profile more than other parameters, for example the influence of multiple reflections. Experimental investigations have shown that for thicker materials and a cutting speed close to the maximum value, the effect of the multiple reflections on the absorptivity becomes important at the bottom part of the cutting front [22].

Based on the cutting profiles we next analyze the absorptivity profiles. For a focal position of f/d=-0.33 the minima of the absorptivity curves for the CO_2 and disk laser are located in the upper part of the work piece. In this case the absorptivity for the CO_2 laser is larger than the absorptivity for the disk laser along most parts of the cutting profile. Only at the top and the bottom part of the cutting profile the situation is reversed. For a focal position of f/d=-0.66 the absorptivity profiles are very similar, however, the curves are shifted towards the bottom surface of the work piece. The minima of the computed absorptivity curves for both lasers are found to coincide approximately with the position of the beam focus. The same general behavior can be observed in the experimental absorptivity curves as shown in Fig. 9 of reference [1]. The experimental absorptivity curve for the disk laser also shows a minimum approximately at the middle of the work piece. The experimental curve for the CO_2 laser shows minima towards the upper and lower part of the work piece but also a minimum at about a depth of 3 mm. The high frequency fluctuations in the experimental absorptivity curves are most likely due to hydrodynamic instabilities. Since the Niziev model assumes that the molten material is removed instantaneously from the kerf those fluctuations cannot be reproduced by the computed curves. Overall however, we find a good agreement between the theoretical and experimental absorptivity curves. By comparing the absorptivity profiles with the corresponding angle of incidence profiles we find that the maxima of the absorptivity profiles are located in regions of the cutting front where the incidence angle is comparable to the Brewster angle.

Finally, we analyze the absorbed intensity profiles which are derived from the absorptivity profiles by insertion of the local angle of incidence. It is important to point out that, despite the CO_2-laser absorptivity being higher than the disk laser absorptivity for most parts of the cutting profile, the corresponding absorbed intensity is higher for the disk laser along the entire cutting profile. This is the main reason why the cutting speed of the disk laser is higher than the cutting speed of the CO_2-laser. For a focal position around the middle of the work piece the situation is reversed for thicknesses in the range of 5 mm to 10 mm. It is worthwhile noting that the absorbed intensity is constant along the entire cutting profile. This, however, is not surprising since we analyzed the stationary solutions and stationary implies that the same amount of material must be removed per unit time at every point along the cutting profile.

4. Conclusions

We present a comparative theoretical analysis of laser cutting of metals at 1 and 10 µm based on the solution of the basic Niziev equation and an extension which incorporates losses due to heat conduction. Generally, we found a qualitative agreement between the basic model and experimental results published elsewhere. Discrepancies observed on absolute scales can be understood by considering the assumptions made in the derivation of Niziev's original model. When incorporating heat conduction we find excellent quantitative agreement. By analyzing the general features of the absorptivity curves and, more importantly, the absorbed intensities along the cutting profiles we find clear indications why the disk laser performs better than the CO_2 laser in a large parameter range. The energy transfer is more effective for the disk laser. In summary, we conclude that the extended Niziev model is very successful in quantitatively explaining some of the discrepancies observed in laser fusion cutting at 1 µm and 10 µm wavelengths.

References

[1] L. D. Scintilla, L. Tricarico, A. Mahrle, A. Wetzig, and E. Beyer., “A comparative study of cut front profiles and absorptivity behavior for disk and CO2 laser beam inert gas fusion cutting.,” *Journal of Laser*

Applications, vol. 42, no. 5, pp. 052006--1, 2012.

[2] K. Hirano and R. Fabbro, “Possible explanations for different surface quality in laser cutting with 1 and 10 µm beams.,” *Journal of Laser Applications,* vol. 24, no. 1, pp. 012006--1,, 2012.

[3] A. Mahrle and E. Beyer., “Theoretical aspects of fibre laser cutting.,” *J. Phys. D: Appl. Phys,* p. 175597, 2009.

[4] F. O. Olsen, “Laser cutting from CO2 laser to disc or fiber Laser Possibilities and challenges.,” in *ICALEO 2011 Congress Proceedings*, Orlando, FL, 2011.

[5] D. Petring, T. Molitor, F. Schneider, and N. Wolf, “Diagnostics, modeling and simulation: Three keys towards mastering the cutting process with fiber, disk and diode lasers.,” *em Physics Procedia ,* vol. 39, pp. 186--196, 2012.

[6] M. Vicanek, G. Simon, H. M. Urbassek, and I. Decker., “Hydrodynamical instability of melt flow in laser cutting.,” *em J. Phys. D: Appl. Phys.,* vol. 20, pp. 140--145, 1987.

[7] C. Wandera, A. Salminen, and V. Kujanpaa, “Inert gas cutting of thick-section stainless and medium-section aluminum using a high power fiber laser,” *Journal of Laser Applications,* vol. 21, no. 3, pp. 154--161, 2009.

[8] C. Wandera and V. Kujanpaa, “Characterization of the melt removal rate in laser cutting of thick-section stainless steel,” *Journal of Laser Applications,* vol. 22, no. 2, pp. 62--70, 2010.

[9] M. Vicanek and G. Simon, “Momentum and heat transfer of an inert gas jet to the melt in laser cutting,” *J. Phys. D: Appl. Phys.,* vol. 20, pp. 1191--1196, 1987.

[10] M. Sparkes, M. Gross, S. Celotto, T. Zhang, and W. O’Neill, “Inert cutting of medium section stainless steel using a 2.2 kw high brightness fibre laser,” in *ICALEO 2006 Congress Proceedings, pages 197--205, Orlando,*, Orlando, FL, 2006.

[11] A. Riveiro, F. Quintero, F. Lusquiños, J. Pou, A. Salminen, and V. Kujanpaa, “Influence of assist gas in fibre laser cutting of aluminum-copper alloy,” in *ICALEO 2008 Congress Proceedings*, Orlando, FL, 2008.

[12] L.D. Scintilla and L. Tricarico, “Estimating cutting front temperature difference in disk and CO2 laser beam fusion cutting.,” *Optics and Laser Technology,* vol. 44, pp. 1468--1479, 2012.

[13] V. G. Niziev, “Theory of CW Laser Beam Cutting,” *Laser Physics,* vol. 3, no. 3, p. 629, 1993.

[14] Michael H. Brügmann and Thomas Feurer, “Comparative theoretical analysis of continuous wave laser cutting of metals at 1 and 10 µm wavelength,” *Applied Physics A,* vol. 116, no. 3, pp. 1353--1364, 2014.

[15] V. G. Niziev and A. V. Nesterov, “Influence of beam polarization on laser cutting efficiency,” *J. Phys. D: Appl. Phys.,* vol. 32, p. 1455, 1999.

[16] P.A. Bélanger and C. Paré, “Optical resonators using graded-phase mirrors,” *Optics Letters,* vol. 16, no. 14, pp. 1057--1059, 1991.

[17] Atanasov, P., “Some aspects of high pressure N2-assisted CO2 laser cutting of metals,” in *Proc. SPIE 1810, 9th International Symposium on Gas Flow and Chemical Lasers*, 1993.

[18] Dell'Erba, M. G. Daurelio, and M. Ferrara, “CO2 laser cutting process of thick aluminium,” *Applied Physics Communications,* vol. 5, no. 1-2, pp. 23--35, 1985.

[19] M. G. Daurelio, Dell'Erba, and L. Cento, “Cutting copper sheets by CO2 laser,” *Lasers and Applications,* pp. 59--64, 1986.

[20] S. Stelzer, A. Mahrle, A. Wetzig, and E. Beyer, “Experimental investigations on fusion cutting stainless steel with fiber and CO2 laser beams,” *Physics Procedia,* vol. 41, pp. 392--397, 2013.

[21] L.D. Scintilla, L. Tricarico, A. Wetzig, and E. Beyer., “Investigation on disk and CO2 laser beam fusion cutting differences based on power balance equation,” *International Journal of Machine Tools and Manufacture,* vol. 69, pp. 30--37, 2013.

[22] L.D. Scintilla, L. Tricarico, A. Wetzig, A. Mahrle, and E. Beyer., “Primary losses in disk and CO2 laser beam inert gas fusion cutting,” *Journal of Material Processing Technology,* vol. 211, pp. 2050--2061, 2011.